Contact Models in Robotics: a Comparative Analysis

Quentin Le Lidec^{1,†}, Wilson Jallet^{1,2}, Louis Montaut^{1,3}, Ivan Laptev¹, Cordelia Schmid¹, and Justin Carpentier¹

Abstract-Physics simulation is ubiquitous in robotics. Whether in model-based approaches (e.g., trajectory optimization), or model-free algorithms (e.g., reinforcement learning), physics simulators are a central component of modern control pipelines in robotics. Over the past decades, several robotic simulators have been developed, each with dedicated contact modeling assumptions and algorithmic solutions. In this article, we survey the main contact models and the associated numerical methods commonly used in robotics for simulating advanced robot motions involving contact interactions. In particular, we recall the physical laws underlying contacts and friction (i.e., Signorini condition, Coulomb's law, and the maximum dissipation principle), and how they are transcribed in current simulators. For each physics engine, we expose their inherent physical relaxations along with their limitations due to the numerical techniques employed. Based on our study, we propose theoretically grounded quantitative criteria on which we build benchmarks assessing both the physical and computational aspects of simulation. We support our work with an open-source and efficient C++ implementation of the existing algorithmic variations. Our results demonstrate that some approximations or algorithms commonly used in robotics can severely widen the reality gap and impact target applications. We hope this work will help motivate the development of new contact models, contact solvers, and robotic simulators in general, at the root of recent progress in motion generation in robotics.

Index Terms—Physical simulation, Numerical optimization.

I. INTRODUCTION

MULATION is a fundamental tool in robotics. Control algorithms, like trajectory optimization (TO) or model predictive control (MPC) algorithms, rely on physics simulators to evaluate the dynamics of the controlled system. Reinforcement Learning (RL) algorithms operate by trial and error and require a simulator to avoid time-consuming and costly failures on real hardware. Robot co-design aims at finding optimal hardware design and morphology and thus extensively rely on simulation to prevent tedious physical validation. In practice, roboticists also usually perform simulated safety checks before running a new controller on their robots. These applications are evidence for a wide range of research areas in robotics where simulation is critical.

To be effective and valuable in practice, robot simulators must meet some fidelity or efficiency levels, depending on the use case. For instance, trajectory optimization algorithms, *e.g.* iLQR[1] or DDP [2], [3], use physics simulation to evaluate the

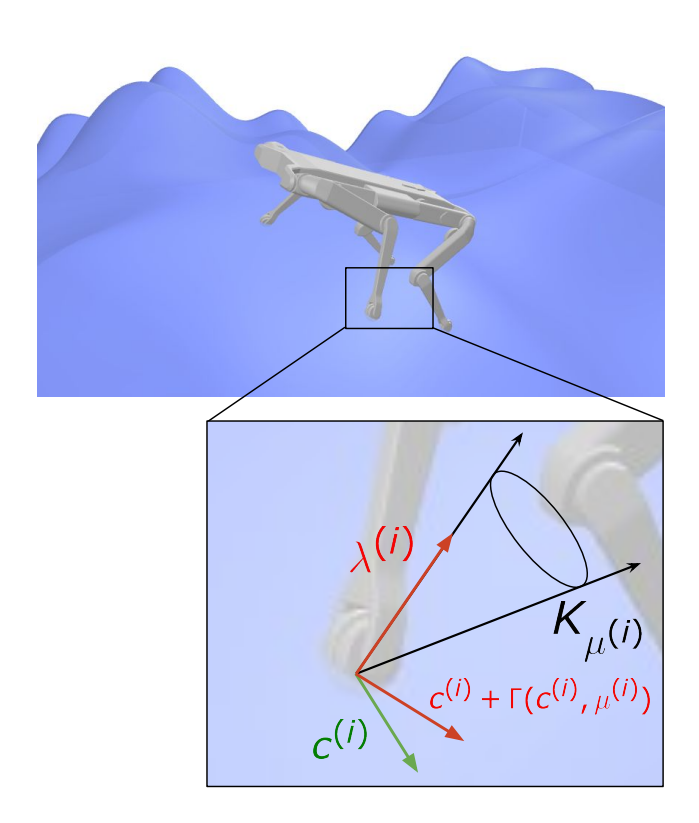


Fig. 1. Illustration of the dynamics of frictional contacts between rigid bodies which are governed by the Signorini condition, the Coulomb's law, and the maximum dissipation principle. The combination of these three principles leads to the Non-linear Complementarity Problem (14).

system dynamics and leverage finite differences or the recent advent of differentiable simulators [4], [5], [6], [7], [8] to compute derivatives. If the solution lacks precision, the real and planned trajectories may quickly diverge, impacting de facto the capacity of such control solutions to be deployed on real hardware. To absorb such errors, the Model Predictive Control (MPC) [9], [10] control paradigm exploits state feedback by repeatedly running Optimal Control (OC) algorithms at high-frequency rates (e.g., 1kHz) [11], [12]. The frequency rate is one factor determining the robustness of this closedloop algorithm to modeling errors and perturbations; thus, the efficiency of the simulation becomes critical. Although RL [13] is considered as a model-free approach, physical models are still at work to generate the samples that are indispensable for learning control policies. In fact, the vast number of required samples is the main bottleneck during training, as days or years of simulation, which corresponds to billions of calls to a simulator, are necessary [14], [15], [16]. Therefore, the efficiency of the simulator directly determines

¹Inria - Département d'Informatique de l'École normale supérieure, PSL Research University. Email: firstname.lastname@inria.fr

²LAAS-CNRS, 7 av. du Colonel Roche, 31400 Toulouse

³Czech Institute of Informatics, Robotics and Cybernetics, Czech Technical University, Prague, Czech Republic

[†]Corresponding author

the computational and, thus, the energetic cost of learning a control policy. Physical accuracy plays an important role after training as well, as more physically accurate simulations will result in a smaller reality-gap to cross for the learned policy to transfer to a real robot [14].

Many manipulation tasks can be tackled by assuming quasistaticity and by considering only a restricted variety of contact events [17], [18]. The recent robotics efforts, highlighted, for instance, by the athletic motions performed by the humanoid robots of Boston Dynamics [19], focus on very dynamic tasks for which these simplification hypotheses cannot hold. In fact, tasks like agile locomotion or dexterous manipulation require the robot to quickly plan and finely exploit, at best, the contact interactions with its environment to shape the movements [20], [21], [22]. In this respect, the ability to handle impacts and frictions, physical phenomena at the core of contact interactions, becomes fundamental for robotic simulators.

Physics simulation is often considered a solved problem with several well-known simulators which are available offthe-shelf. However, simulating a physical system raises several and complex issues that are usually circumvented at the cost of approximations or costly computation. When simulating a system evolving freely, rigid body dynamics algorithms [23], [24] are now established as the way to go due to their high efficiency. For robotics, one has to consider interactions through contact between the robot and its environment, thus constraining the movement. However, due to the creation or the breaking of contacts along a trajectory, the dynamics switch from one mode to the other, making the problem of simulating a system with contacts and frictions highly non-smooth and non-convex [25], [26], [27]. More precisely, contact dynamics between rigid objects are governed by three main principles: the Signorini condition specifies the unilaterality nature of contact interactions, while the Coulomb's law of friction and the maximum dissipation principle (MDP) of Moreau state that friction force should lie inside a second-order cone and oppose the movement.

Altogether, these three principles correspond to a so-called nonlinear complementarity problem (NCP), which is nonconvex and thus difficult to solve in general [28]. Numerical methods to solve this NCP fall into two main categories: event-driven and time-stepping methods [28]. Most modern robotics simulators are part of the latter category because predicting collisions is intractable due to the complexity of the scenes. Therefore, we will restrain our study to this type of method. Historically, the Open Dynamic Engine (ODE)[29] is one of the first open-source simulators with a large impact on the community, which was then followed by Bullet [30]. Both of them rely on maximal coordinates to depict the state of the objects and kinematic constraints imposed by the articulations are tackled explicitly. Such a choice leads to large-dimensional problems to solve, impacting de facto the computational performances. To lower the computational burden, alternative simulators rooted in generalized coordinates, like DART [31] and MuJoCo [32], appeared shortly after. More recently, RaiSim [33] emerged as one of the first simulators enabling RL policies to transfer to real quadrupedal robots. Its implementation being closed source, we provide what constitutes, to the best of our knowledge, the first in-depth study and open-source re-implementation of this contact solver. Still today, the number of alternative algorithms available is growing fast [34], [6], [8]. In general, these simulators differ at their very core: one should be aware of the contact modeling embedded in the simulator they are using and how it can impact the applications they aim at. Some high-level benchmarks of simulators exist [35], evaluating the whole simulation pipeline and its multiple internal routines, e.g. rigid-body dynamics algorithms, collision detection, and contact problem-solving. Our work closely relates to [36]. It separately assesses the various contact models and their associated algorithms. We achieve this by decoupling the contact models from their implementations and re-implemented the solvers with a unique back-end based on the Pinocchio toolbox [24], [37] for evaluating the dynamic quantities and on HPP-FCL [38], [39], [40] for computing the collisions. We pursue the effort of [36] by studying recent algorithms and adding advanced evaluation criteria. Our experiments are done in both illustrative and realistic robotics setups.

We made the following contributions:

- → we make a detailed survey of contact models and their associated algorithms, including established and more recent robotics simulators;
- → we develop an open source and generic implementation
 of the main robotic contact solvers in C++;
- ⇒ based on our implementation and the theoretical study, we propose quantitative criteria which allow performing an in-depth evaluation of both physical and computational aspects of contact models and solvers.
- → we explore the impacts of the simulation choices on the practical application of MPC for quadruped locomotion.

The article is organized as follows: we first recall the background of contact simulation: the physical principles behind contact modeling (Sec. II) and the numerical algorithms allowing us to solve the resulting equations (Sec. III). In the experimental part (Sec. IV), we propose an exhaustive empirical evaluation of the various existing contact models and solvers to assess both their physicality (Sec. IV-A) and computational efficiency (Sec. IV-C). At last, Sec. IV-D investigates the consequences of the contact models in the context of quadruped locomotion. It is finally worth mentioning that the authors are linked to the Pinocchio and HPP-FCL open-source projects.

II. RIGID CONTACT MODELLING

We start by stating the physical principles commonly admitted for rigid body simulation with point contact. If these principles remain hypothetical and can still be discussed, they have been, in general, empirically tested and are arguably better than their relaxations. Once the modeling is done, we transcribe these physical laws into a numerical problem, which should be solved via optimization-based techniques to simulate a system with contacts and frictions. We also present the various open-source tools that allow computing all the intermediate quantities necessary to build a physics simulator.

In this paper, we describe the state of a system with its generalized coordinates $q \in \mathcal{Q} \cong \mathbb{R}^{n_q}$. We denote by $v \in \mathcal{TQ} = \mathbb{R}^{n_v}$ the joint velocity.

Free motion. The principle of least action states that the path followed by a dynamical system should minimize the action functional [41]. This principle induces the celebrated Lagrangian equations of motion:

$$M(q)\dot{v} + C(q, v)v + g(q) = \tau \tag{1}$$

where $M \in R^{n_v \times n_v}$ represents the joint space inertia matrix of the system, C(q,v)v accounts for the centrifugal and Coriolis effects, and g is the generalized gravity. This Lagrangian equation of motion naturally accounts for the kinematic constraints induced by the articulations of the rigid-body dynamical system. When applied to a robot, *i.e.*, a system of multiple rigid bodies, the inertia matrix M becomes sparse. Rigid body dynamic algorithms exploit this sparsity at best [23], [24] making it possible to compute the free acceleration in less than $4\mu s$ for the robots as complex as a 36-dof humanoid. As done by time-stepping approaches [28], we will express the problem in terms of velocities rather than acceleration, thus discretizing (1) into:

$$Mv^{t+1} = Mv^t + (\tau - Cv - g)\Delta t.$$
 (2)

We note v^f the free velocity which is defined as the solution of (2).

Bilateral contact. When the system is subject to constraints, *e.g.* kinematic loop closures or anchor points, it is convenient to represent them implicitly:

$$\Phi(q) = 0. (3)$$

where $\Phi: \mathbb{R}^{n_q} \mapsto \mathbb{R}^m$ is the implicit constraint function of dimension m, which depends on the nature of the constraint. For resolution, it is more practical to proceed to an index reduction [42] by deriving w.r.t. time (3) to express it as a constraint on joints velocities:

$$c - c^* = 0. (4)$$

where $c=Jv^{t+1}$ is the constraint velocity, $J=\partial\Phi/\partial q$ is the constraint Jacobian which can be computed efficiently via the rigid body dynamics algorithms [23], [43] and c^* is the reference velocity of the constraint. Such a constraint (7) is enforced by the action of the environment on the system via the contact vector impulse $\lambda \in \mathbb{R}^m$. These considerations lead to Gauss's principle of least constraint [44], [45], *i.e.* the acceleration of a constrained physical system is as similar as possible to that of the unconstrained system. By duality, the contact impulses are spanned by the adjoint of the constraint Jacobian and should be incorporated in the Lagrangian equations (2) via:

$$Mv^{t+1} = Mv_f + J^{\top}\lambda \tag{5}$$

Regarding bilateral contacts, the contact efforts, corresponding to the Lagrange multipliers associated with the constraint (3), are unconstrained. If a bilateral constraint is well

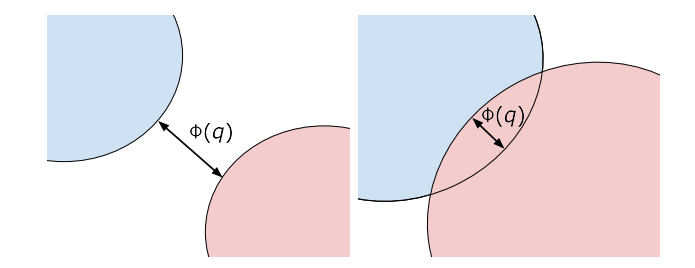


Fig. 2. The separation vector Φ allows to formulate the non-penetration constraint which leads to the *Signorini condition* (8). This vector is computed by the GJK or EPA algorithms which are internal blocks of the simulator. We refer to [46] for a tutorial introduction on the topic.

suited to model kinematic closures, it is not to model interactions between the robot and its environment, which are better represented by unilateral contacts. This paper focuses on the latter, for which we provide a more detailed presentation.

Unilateral contact. When a system is in contact with its environment, the rigid body hypothesis enforces the normal component of the separation vector between the two objects [40], *i.e.* the signed distance function, to be non-negative. Expanding the bilateral case, the constraint function Φ now coincides with the separation vector (Fig. 2) and describes a unilateral constraint:

$$\Phi(q)_N \ge 0 \tag{6}$$

where $\Phi(q) \in \mathbb{R}^{3n_c}$, n_c is the number of contacts and the subscripts N and T respectively account for the normal and tangential components. In practice, Φ can be computed efficiently via the Gilbert-Johnson-Keerthi (GJK) [47], [40] and the Expanding Polytope Algorithm (EPA) algorithms[48]. In order to ease the resolution, one can write (6) in terms of velocities, and the Taylor expansion of this condition leads to:

$$c_N - c_N^* \ge 0 \tag{7}$$

where $c=Jv^{t+1}\in\mathbb{R}^{3n_c}$ is the velocity of contact points. We explain later how c_N^* is set to model physical effects or improve the numerical accuracy of the solutions. As in the bilateral case, the adjoint operator of the contact Jacobian J spans the contact forces, which leads again to (5) the constrained equations of motion. Unlike the bilateral case, unilateral contacts constrain the possible efforts λ . In a frictionless situation, the tangential forces are null, which implies that $\lambda_T=0$. In addition, the contact forces λ can only be repulsive as they should not act in a glue-like fashion (the environment can only push and not pull on the feet of a legged robot) and, thus, are forced to be non-negative. An impulse cannot occur when an object takes off, i.e., the normal velocity and impulse cannot be non-null simultaneously. Combining these conditions, we obtain the so called Signorini condition [49]:

$$0 \le \lambda_N \perp c_N - c_N^* \ge 0. \tag{8}$$

However, such a condition does not define a mapping between λ_N and c_N , *i.e.* the contact forces are not a function of the penetration error. Indeed, its representation is an infinitely steep graph that may be relaxed into a mapping via a spring

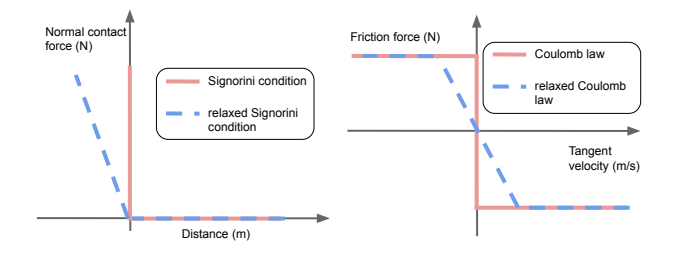


Fig. 3. Both the Signorini condition (Left) and the Coulomb's law (Right) induce infinitely steep graphs, which make the contact problem hard to solve.

damper accounting for local deformation of the materials (see Fig. 3). Substituting, v^{t+1} by its expression from the Lagrangian equations (5), we obtain a Linear Complementarity Problem (LCP) [50]:

$$0 \le \lambda_N \perp (G\lambda + g)_N - c_N^* \ge 0 \tag{9}$$

where $G = JM^{-1}J^{\top}$ is the so-called Delassus matrix, and $g = Jv^f$ is the free velocity of contact points (the velocity of the contact points in the unconstrained cases). It is worth mentioning at this stage that several approaches [23], [51], [43] have been developed in the computational dynamics and robotics literature to efficiently evaluate the Delassus matrix.

In the case of rigid bodies - purely inelastic impacts, and exact collision detection, i.e. $\Phi(q)_N = 0$ - the reference velocity c_N can be set to 0. However, setting this velocity to a non-null quantity may be useful to improve the modeling on both physical and numerical aspects. A first benefit is a possibility of accounting for impacts that may occur when two objects collide with non-null relative normal velocity. The most common impact law stipulates $c^* = -ec^t$ where e is the restitution coefficient which adjusts the quantity of energy dissipated during the collision. Another benefit is when time stepping methods are employed, one cannot avoid penetration errors, i.e. $\Phi(q)_N < 0$, but it is possible to prevent these errors from growing over time via a Baumgarte correction [52] which sets $c^* = K \max(0, -\Phi(q)_N)$. In addition, in most cases in robotics, the Delassus' matrix G is rank deficient. Such physical systems are said to be hyperstatic, and because rank $(J) > n_v$, several λ values may lead to the same trajectory. This under-determination can be circumvented by relaxing the rigid-body hypothesis, i.e. the Signorini condition, and considering compliant contacts via a reference velocity linearly depending on λ as represented in Fig. 3 Indeed, with $c^* = -R\lambda$ where R is a diagonal matrix with non-null and positive elements only on the normal components, called compliance and whose value is a property of the material, the original Delassus matrix G is replaced by the damped matrix $\tilde{G} = G + R$ which is full rank.

Friction phenomena are at the core of contact modeling as they precisely allow manipulation or locomotion tasks. Coulomb's law for dry friction represents the most common way to model friction forces. This phenomenological law states that the friction forces λ_T should be proportional to the normal contact forces λ_N and the friction coefficient μ . Mathematically,

this suggests that contact forces should lie inside an ice cream cone whose aperture is set by the coefficient of friction μ :

$$\lambda \in K_{\mu} = \prod_{i=1}^{n_c} K_{\mu^{(i)}} \tag{10}$$

where the superscript (i) refers to the i^{th} contact point and $K_{\mu^{(i)}} = \{\lambda | \lambda_N \geq 0, \|\lambda_T\|_2 \leq \mu^{(i)} \lambda_N \}$. Additionally, when sliding occurs, the maximum dissipation principle formulated by Jean-Jacques Moreau [25] implies that the frictional forces should maximize the dissipated power:

$$\forall i, \ \lambda_T^{(i)} = -\mu^{(i)} \lambda_N^{(i)} \frac{c_T^{(i)}}{\|c_T\|}, \text{if } \|c_T^{(i)}\| > 0.$$
 (11)

As for the Signorini condition, Coulomb's law does not describe a mapping but an infinitely steep graph (Fig. 3). Relaxing this law via viscous frictions, *i.e.* assuming the tangent contact forces to be proportional to the tangent velocities, allows defining a mapping between λ_T and c_T .

Combining the Coulomb's law for friction with the *Signorini* condition evoked earlier, we finally get three distinct cases corresponding to a sticking contact point (12a), a sliding contact point (12c) or a take-off (12b):

$$\begin{cases} \lambda^{(i)} \in K_{\mu^{(i)}}, \text{if } c^{(i)} = 0 & \text{(12a)} \\ \lambda^{(i)} = 0, \text{if } c_N^{(i)} > 0 & \text{(12b)} \\ \lambda^{(i)} \in \partial K_{\mu^{(i)}}, \exists \alpha > 0, \lambda_T^{(i)} = -\alpha c_T^{(i)} \text{ otherwise.} & \text{(12c)} \end{cases}$$

where ∂K indicates the border of the cone. The equations (12) are referred to as the disjunctive formulation of the contact problem. However, such a formulation is not suited for solving as the switching condition depends on the contact point velocity c. As this quantity is an unknown of the problem, one cannot know in which case of (12) they are standing. For this reason, the problem is often reformulated as a nonlinear complementarity problem (NCP). Indeed, using de Saxcé's bipotential function [53] defined as:

$$\Gamma: (c, \mu) \in \mathbb{R}^3 \times \mathbb{R} \mapsto [0, 0, \mu \|c_T\|_2]$$
(13)

one can show that (12) is equivalent to the following [27], [54] (Fig. 1):

$$\forall i, K_{\mu^{(i)}} \ni \lambda^{(i)} \perp c^{(i)} + \Gamma\left(c^{(i)}, \mu^{(i)}\right) \in K_{\mu^{(i)}}^*.$$
 (14)

In (14), K_{μ}^* refers to the dual cone of K_{μ} such that if $\lambda \in K_{\mu}$ and $c \in K_{\mu}^*$, then $\langle \lambda, c \rangle \geq 0$, where $\langle \cdot, \cdot \rangle$ is the canonical scalar product.

Eq. (14) allows to define, for each contact $i \in [\![1,n_c]\!]$, the primal and dual residuals as $\epsilon_p^{(i)} = \operatorname{dist}_{K_{\mu^{(i)}}} \left(\lambda^{(i)}\right)$ and $\epsilon_d^{(i)} = \operatorname{dist}_{K_{\mu^{(i)}}} \left(c^{(i)} + \Gamma\left(c^{(i)},\mu^{(i)}\right)\right)$ respectively, where $\operatorname{dist}_{\mathcal{C}}$ is the distance function w.r.t. a convex set \mathcal{C} . It also induces a contact complementarity criterion $\epsilon_c^{(i)} = \left|\langle \lambda^{(i)}, c^{(i)} + \Gamma\left(c^{(i)},\mu^{(i)}\right)\rangle\right|$. From these per-contact criteria, it is then possible to introduce a well-posed absolute convergence criterion ϵ_{abs} for (14), as the maximum of $\epsilon_p^{(i)}, \epsilon_d^{(i)}$ and $\epsilon_c^{(i)}$ for all i. We use this criterion as a stopping criterion in our implementation of NCP solvers, but also as a measure of physical accuracy in our experiments of Section IV.

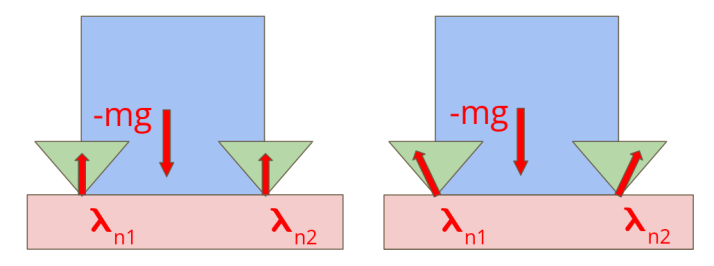


Fig. 4. **Underdetermined contact problem.** The left and right contact forces are solutions of the NCP (14) and lead to the same system velocity. Such an undetermined problem can also occur on normal forces.

At this point, it is worth mentioning that the problem (14), which we refer to as NCP, does not derive from a convex optimization problem, thus making its resolution complex. Alternatively, one can see the frictional contact problem as two interleaved convex optimization problems [34], [55], [6] whose unknowns, λ and v, also define each other problems. Practically, this can induce the existence of multiple, or even an infinite number of contact forces satisfying (14). As mentioned earlier, this can be due to normal forces, but tangential components can also cause under-determination (Fig. 4). Even though it does not impact the trajectories of rigid bodies, a simulator should not exhibit internal forces compressing or stretching the objects. Indeed, such forces would not coincide with the forces observed by force sensors and would rather correspond to some internal deformations of the objects, which should thus be considered soft and no more rigid. Additionally, these internal forces might also be problematic as it is impossible to characterize them. This may induce inconsistent derivatives, which become critical in the context of differentiable simulation.

Open-source frameworks for contact simulation. To conclude this section, we propose to review the main open-source software that has been developed by the robotics community and can be used for simulating contact. Simulating contact interactions, as illustrated in Fig. 5, involved two main stages, corresponding to the collision detection step (which shapes are in contacts) and the collision resolution (which contact forces are applied through the contact interaction). These frameworks are enumerated in Tab. I.

More precisely, at each time step, a simulator must first detect which geometries are colliding and compute their separation vector Φ . The GJK and EPA algorithms are widely adopted for their low computational cost. HPP-FCL [38], [39], [40], the extension of Flexible Collision Library (FCL) [56] and libccd [57] implement them efficiently. Some simulators such as Bullet [30] or ODE [29] also re-implement the same algorithm as an internal routine.

Once collisions are evaluated, one still requires the contact points free velocity v_f and Jacobians J to formulate (14). These two quantities are efficiently computed via the rigid body algorithms [23]. The RBDL [58] or the Pinocchio library [24] provide efficient implementations to evaluate them. In addition, Pinocchio proposes a direct and robust way to compute Cholesky's decomposition of the Delassus' matrix G [43].

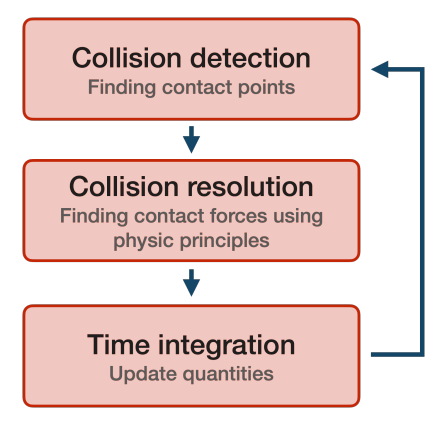


Fig. 5. **Simulation routines.** When simulating rigid bodies with frictional contacts, a physics engine goes through a suite of potentially challenging sub-problems: the collision detection, the collision resolution, and the time integration step.

 $\label{table I} \mbox{TABLE I}$ Open source tools for physics simulation in robotics.

	License	API	Used by		
Collision detection					
FCL [56]	BSD	C++	DART, Drake		
libccd [57]	BSD	C++, Python	MuJoCo, Drake, FCL, Bullet, ODE		
HPP-FCL [38]	BSD	C++, Python	Pinocchio		
Bullet [30]	BSD	C++, Python	DART		
ODE [29]	BSD/GPL	C++, Python	DART		
Rigid body dynamics algorithms					
Pinocchio [24]	BSD	C++, Python			
RBDL [58]	zlib	C++, Python			
Collision resolution					
MuJoCo [32]	Apache 2.0	C++, Python			
DART [31]	BSD 2	C++, Python			
Bullet [30]	BSD	C++, Python			
Drake [59]	BSD 3	C++, Python			
ODE [59]	BSD/GPL	C++, Python			

These algorithms are also embedded as internal routines in various simulators such as MuJoCo [32], DART[31], Drake [59], Bullet [30] or ODE[29].

Eventually, when all quantities necessary to formulate the NCP (14) are computed, the simulator has to call a solver. Every simulator, *i.e.* MuJoCo[32], DART [31], Bullet[30], Drake[59] and ODE[29], proposes its own implementation. This procedure varies greatly depending on the physics engine, as each has its own physical and numerical choices. We detail in the next section the existing algorithms.

III. ALGORITHMIC DERIVATIONS OF THE CONTACT PROBLEM

As explained in the previous section, the nonlinear complementarity problem (14) does not derive from a variational principle. Thus, classical numerical optimization solvers will not be of any help in solving it. This section studies the various approximations and algorithmic techniques in the literature to tackle this problem. As summarized in Tab. II, this section is organized in subsections describing the four contact models most commonly used in robotics, namely the linear complementarity problem (LCP), the cone complementary

	Signorini	Coulomb	MDP	No shift	No internal forces	Robust	Convergence guarantees
LCP							
PGS [30], [29], [60], [31]	/			✓			✓
Staggered projections [34]	✓			✓	✓	✓	
ССР							
PGS [61]		✓	✓	✓			✓
MuJoCo [32]		✓	✓		✓	✓	✓
ADMM (Alg. 3)		✓	✓	✓	✓	✓	✓
RaiSim [33]	✓	1		✓			
NCD							

TABLE II
CHARACTERISTICS OF VARIOUS CONTACT MODELS.

problem (CCP), RaiSim, and the nonlinear complementarity problem (NCP). For each contact model, we also report the related algorithmic variants. If each tick in Tab. II represents a positive point for the concerned algorithm, Sec. IV shows that even one default may be prohibitive and can cause a solver to be unusable in practice. Finally, we also mention a set of useful implementation tricks which should be used to build an efficient simulator.

Staggered projections [6]

Linear Complementarity Problem. A first way to simplify the resolution of problem (14) is to linearize the NCP problem by approximating the second-order cone constraint from Coulomb's law with a pyramid, typically composed of four facets. This is done by replacing $K_{\mu^{(i)}}$ by $\tilde{K}_{\mu^{(i)}} = \left\{ \lambda | \lambda_N \geq 0, \| \lambda_T \|_{\infty} \leq \mu^{(i)} \lambda_N \right\}$. Doing so allows retrieving a linear complementarity problem (LCP), often easier to solve [50]. Such a problem is more standard and betterstudied than its nonlinear counterpart [62]. Indeed, the standard Lemke's algorithm [50] or the projected Gauss-Seidel (PGS) algorithm (Alg. 1) allow to solve it and even come with convergence guarantees. Due to its easy implementation, the PGS algorithm may seem attractive and was widely adopted by modern physics engines, such as in Bullet [30], PhysX [60], ODE [29], and DART [31], [7] simulators.

This iterative algorithm loops on contact points and successively updates the normal and tangent contact forces. Because PGS works separately on each contact point, the update compensates for the current errors due to the estimated forces from other contact points. Yet, as illustrated in the experimental section IV, this process induces the emergence of internal forces during the resolution. Moreover, Gauss-Seidellike approaches are similar to what is also known as block coordinate descent in the optimization literature. As first-order algorithms, they do not benefit from improved convergence rates or robustness with respect to their conditioning, unlike second-order algorithms. In parallel, the linearization of the second-order cone causes the loss of the isotropy for frictions, as stated by Coulomb's law. By choosing the axes for the facets of the pyramid and due to the maximum dissipation principle, one incidentally biases the friction forces towards the corners, as illustrated in Fig. 6. This error is sometimes mitigated by increasing the number of facets which also comes

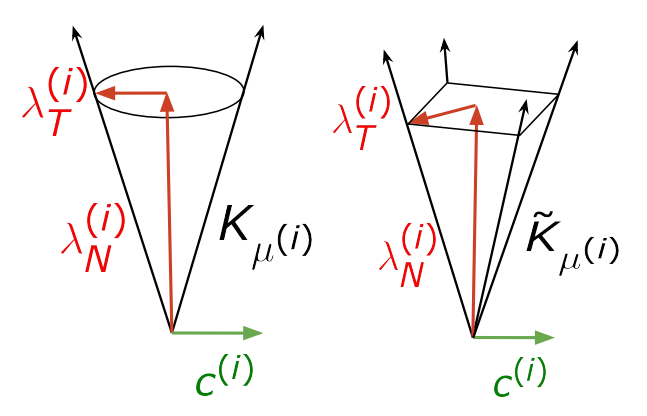


Fig. 6. Cone linear approximation. Linearizing the friction cone induces a bias on the direction of friction forces. The MDP tends to push tangential forces toward the corners of the pyramid.

Algorithm 1: Pseudo-code of the projected Gauss-Seidel (PGS) algorithm for solving LCPs.

Input: Delassus matrix: G, free velocity: g, friction cones K_{μ} Output: Contact forces: λ , velocity: v1 for k=1 to M do

2 | for i=1 to n_c do

3 | $\lambda_N^{(i)} \leftarrow \lambda_N^{(i)} - \frac{1}{G_{iN}} (G\lambda + g)_N^{(i)};$ 4 | $\lambda_N^{(i)} \leftarrow \max(0, \lambda_N^{(i)});$ 5 | $\lambda_T^{(i)} \leftarrow \lambda_T^{(i)} - \frac{1}{\min(G_i, G_i)} (G\lambda + g)_T^{(i)};$ 6 | $\lambda_T^{(i)} \leftarrow \operatorname{clamp}(\lambda_T^{(i)}, \mu_i \lambda_N);$ 7 | end

8 end

at the cost of more computations.

Cone Complementarity Problem. An alternative approach consists in approximating the NCP problem in order to transform it into a more classical convex optimization problem. By relaxing the complementarity constraint from (14), one can obtain a Cone Complementarity Problem (CCP) [61]:

$$K_{\mu} \ni \lambda \perp c \in K_{\mu}^{*} \tag{15}$$

If this relaxation preserves the Maximum Dissipation Principle (MDP) and the second-order friction cone, it loses the *Signorini* condition (8). Indeed, re-writing the complementarity of (15) in the case of a sliding contacts yields:

$$\lambda_N c_N + \lambda_T^\top c_T = 0, \tag{16}$$

and in the case of sliding contact, the MDP leads to:

$$\lambda_N c_N - \mu \lambda_N \|c_T\|_2 = 0, \tag{17}$$

which is equivalent to the following complementarity condition:

$$\lambda_N \perp (c_N - \mu \| c_T \|_2).$$
 (18)

(18) indicates that the CCP approximation allows for simultaneous normal velocity and forces, contrary to (8). The problem (15) can in fact be viewed as the Karush Kuhn Tucker conditions of an equivalent Quadratically Constrained Quadratic Programming (QCQP) problem:

$$\min_{\lambda \in K_u} \frac{1}{2} \lambda^\top G \lambda + g^\top \lambda \tag{19}$$

Once the contact problem is formulated as an optimization problem, any optimization algorithms can be employed to solve it. Here, we propose to study an ADMM algorithm [63] to solve (19), but Interior Point algorithms [64] can be used as in the latest Mujoco's version [32]. A benefit of using the family of proximal algorithms like ADMM is their natural ability to handle ill-conditioned and hyper-static cases. Another byproduct of such methods is the implicit regularization they induce on the found solution, which removes the potential internal forces.

One may argue that such algorithms require to compute G^{-1} (Alg. 3, line 3) while per contact approaches repeatedly solve for each contact point individually, and thus only require the cheap inverse of diagonal blocks from G (Alg. 1, lines 3,5, Alg. 2, line 3, Alg. 4, line 4, Alg. 5, lines 3,5). However, the recent progress [43] demonstrated the Cholesky decomposition of G can be computed efficiently and robustly. We detail this point later when discussing implementation tricks, at the end of this section. Exploiting the knowledge of G^{-1} and not the block components as in the "per-contact" approaches mentioned earlier allows us to capture the coupling between all contact points. The most recent version of MuJoCo [32] adopts this approach with a Newton solver. In parallel, MuJoCo replaces G by $\hat{G} = G + R$ in the quadratic part of (19), which is justified by a compliant contact hypothesis. As evoked earlier, R is homogeneous to a compliance which should be a material property of the objects involved in the collision. However, MuJoCo arbitrarily set this to the diagonal of αG , where $\alpha \in [0,1]$ is close to 0. This choice has no physical justification (at least, without making strong assumptions that are not met in practice), and its only intent is to improve the conditioning of the problem to ease the resolution and artificially make the solution unique. Moreover, R has nonnull tangential components and thus may also introduce some tangential "compliance" which corresponds to the relaxation of Coulomb's law (Fig. 3). In fact, this should instead be interpreted as a Tikhonov regularization term enforcing the

Algorithm 2: Projected Gauss-Seidel (PGS) algorithm for Cone Complementarity Problem (CCP)

Input: Delassus matrix: *G*, free velocity: *g*, friction

```
Output: Contact forces: \lambda, velocity: v

1 for k = 1 to M do

2 | for i = 1 to n_c do

3 | \lambda^{(i)} \leftarrow \lambda^{(i)} - \frac{3}{G_i + G_i + G_i} (G\lambda + g)^{(i)};

4 | \lambda^{(i)} \leftarrow \operatorname{proj}_{K_{\mu_i}}(\lambda^{(i)});

5 | end

6 end
```

Algorithm 3: ADMM algorithm for Cone Complementarity Problem (CCP)

Input: Delassus matrix: G, free velocity: g, friction cones K_{μ} Output: Contact forces: λ , velocity: v1 $\tilde{G}^{-1} \leftarrow (G + \rho \operatorname{Id})^{-1}$;

2 for k = 1 to M do

3 $\lambda \leftarrow -\tilde{G}^{-1}(g - \rho z + \gamma);$ 4 $z \leftarrow \operatorname{proj}_{K_{\mu}}(\lambda + \frac{\gamma}{\rho});$ 5 $\gamma \leftarrow \gamma + \rho(\lambda - z);$

strict convexity of the problem to facilitate the numerics and the existence of both the forward and inverse dynamics computation at the cost of shifting, even more, the solution.

RaiSim contact model. A contact model introduced in [65] and implemented in the RaiSim simulator [33] aims at partially correcting the drawbacks from the CCP contact model exploited in MuJoCo [32]. As explained earlier, the CCP formulation relaxes the Signorini condition for sliding contacts, leading to positive power from normal contact forces. The contact model proposed in [65] fixes this by explicitly enforcing the Signorini condition by constraining $\lambda^{(i)}$ to remain in the null normal velocity hyper-plane $V_N^{(i)} = \{\lambda | G_N^{(i)} \lambda + g_N^{(i)} = 0\}$. For a sliding contact point, the problem (19) becomes:

$$\min_{\lambda \in K_{\mu^{(i)}} \cap V_N^{(i)}} \frac{1}{2} \lambda^\top G^{(i)} \lambda + \tilde{g}^{(i)\top} \lambda \tag{20}$$

where $\tilde{g}^{(i)}=g^{(i)}+\sum_{j\neq i}G_{ij}\lambda^{(j)}$ is the ith contact point velocity as it was free. The new problem (20) remains a QCQP and [33] leverages the analytical formula of the ellipse $K_{\mu^{(i)}}\cap V_N^{(i)}$ in polar coordinates to tackle it as a 1D problem via the bisection algorithm [66] (Alg. 4, line 10). We refer to the original publication for a more detailed description of the bisection routine [33].

This approach implies several drawbacks. Indeed, it requires knowing whether a contact point is sliding, which cannot be known in advance as the contact point velocity depends on the contact forces. Thus, some heuristics, based on the disjunctive formulation of the contact problem (12), are introduced to try to guess the type of contact which will occur, *i.e.* take-off (Alg. 4,

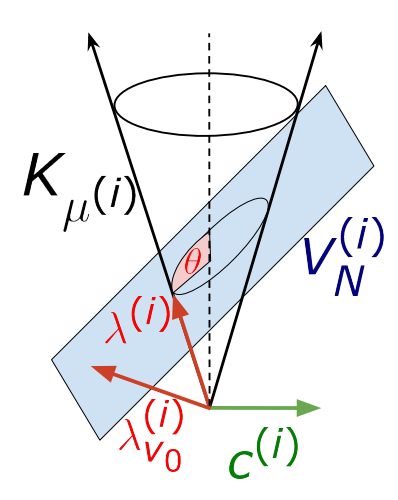


Fig. 7. **Bisection algorithm.** When the contact point is sliding, $\lambda_{v_0}^{(i)}$ (Alg. 4, line 4) lies outside of the friction cone $K_{\mu^{(i)}}$, leading to a non-null tangential contact velocity $e^{(i)}$. In this case, RaiSim solves (20). This is equivalent to finding the $\lambda \in K_{\mu^{(i)}} \cap V_N^{(i)}$ which is the closest to $\lambda_{v_0}^{(i)}$ under the metric defined by $G^{(i)}$. The constraint set being an ellipse, the problem boils down to a 1D problem on θ using polar coordinates. This figure is inspired from Fig. 2 of [33].

line 5), sticking (Alg. 4, line 7) or sliding (Alg. 4, line 9). Obviously, such heuristics may be wrong, which may cause the algorithms to get stuck and lose convergence guarantees. This effect is strengthened by the caveats of the per-contact loop, which additionally make RaiSim not robust to conditioning and prone to internal forces. Eventually, if adding the constraint $\lambda^{(i)} \in V_N^{(i)}$ allows to retrieve the Signorini condition from the CCP model, it also induces the loss of the maximum dissipation principle. Writing the Karush Kuhn Tucker (KKT) conditions of the problem (20) and some algebra manipulations yields:

$$c_T^{(i)} \propto -\lambda_T^{(i)} - \frac{{\mu^{(i)}}^2 \lambda_N^{(i)}}{G_{NN}^{(i)}} G_{NT}^{(i)}$$
 (21)

which contradicts (11).

Tackling the NCP. Despite the non-smooth and non-convex issues described previously, some simulation algorithms aim to directly solve the original NCP problem [67], [54]. The PGS algorithm exploited for LCP and CCP problems can easily be adapted to the NCP case by changing the clamping step (Alg. 1,line 6) or the normal projection (Alg. 2, line 4) for a horizontal projection on the cone (Alg. 5, line 6). However, it is worth noting that such approaches have fewer convergence guarantees than their relaxed counterpart [27]. As with every Gauss-Seidel approach, the methods inherited from the sensitivity to ill-conditioning and spurious internal forces. The staggered projections [34], [6] (Alg. 6) approach proceeds by rewriting the NCP as two interleaved optimization problems. This interconnection is solved via a fix-point algorithm that repeatedly injects one problem's solution into the formulation of the other. The staggered projections algorithm has no convergence guarantees but was heavily tested and seems, in practice, to converge most of the time in a few iterations (typically five iterations [6]). However, solving a cascade of

Algorithm 4: Per-contact bisection algorithm

```
Input: Delassus matrix: G, free velocity: g, friction
               cones K_{\mu}
    Output: Contact forces: \lambda, velocity: v
 1 for k=1 to M do
         for i=1 to n_c do
              3
 4
 5
 6
               else if \lambda_{v_0}^{(i)} \in K_{\mu^{(i)}} then // stiction
 7
 8
 9
                    // sliding
                    \lambda^* \leftarrow \text{bisection}(G_{ii}, \tilde{g}^{(i)}, K_{u^{(i)}}, \lambda_{v_0}^{(i)});
10
11
               \lambda^{(i)} \leftarrow \alpha \lambda^{(i)} + (1 - \alpha) \lambda^*;
12
               \alpha \leftarrow \gamma \alpha + (1 - \gamma) \alpha_{min}
13
         end
14
15 end
```

Algorithm 5: Projected Gauss-Seidel (PGS) algorithm for Non-linear Complementarity Problem (NCP)

```
Input: Delassus matrix: G, free velocity: g, friction cones K_{\mu}

Output: Contact forces: \lambda, velocity: v

1 for k=1 to M do

2 | for i=1 to n_c do

3 | \lambda_N^{(i)} \leftarrow \lambda_N^{(i)} - \frac{1}{G_{iN}} (G\lambda + g)_N^{(i)};

4 | \lambda_N^{(i)} \leftarrow \max(0, \lambda_N^{(i)});

5 | \lambda_T^{(i)} \leftarrow \lambda_T^{(i)} - \frac{1}{\min(G_i, G_i)} (G\lambda + g)_T^{(i)};

6 | \lambda_T^{(i)} \leftarrow proj_{\mu_i \lambda_N^{(i)}} (\lambda_T^{(i)});

7 | end

8 end
```

optimization problems allows the use of robust optimization algorithms (*e.g.*, ADMM), but remains more costly than other approaches.

Additional practical tricks. In practice, the performances of contact solvers can be improved by a few simple tricks. The most important one is warm-starting the solver by providing the contact forces from the previous time step. Indeed, in the case of a persisting contact between two objects, the contact forces can be cached and reused as an initial guess when solving for the contact forces of the next-time step. This relies on the ability of the contact solver algorithm to be warm-started. This excludes Interior Point algorithms as they expect a feasible initial guess. In contrast, the feasible set of contact forces may change from one time step to the other, even in the case of a persisting contact point. On the opposite, augmented lagragian (AL) methods can naturally be warm started: not only the

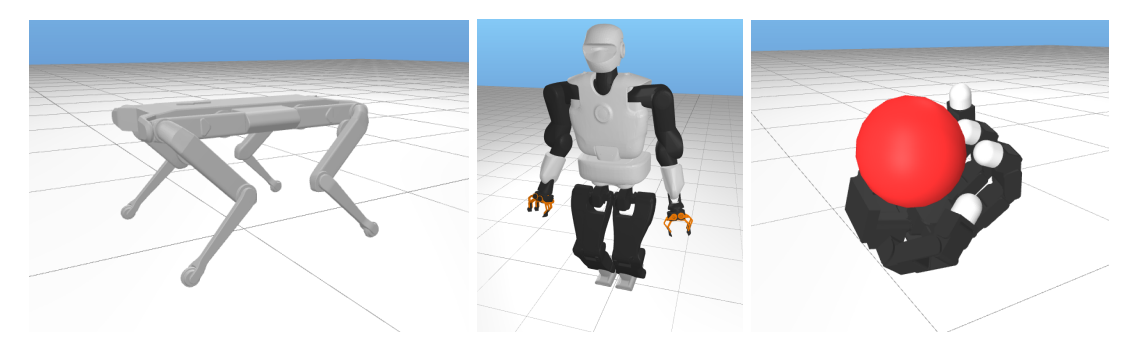


Fig. 8. Robotics systems used for the experiments. The Solo-12 quadruped (Left), the Talos humanoid (Center) and the Allegro hand (Right) allow to respectively exhibit locomotion, high-dimensional, and manipulation contact scenarii.

```
Algorithm 6: Staggered projections algorithm

Input: Delassus matrix: G, free velocity: g, friction cones K_{\mu}

Output: Contact forces: \lambda, velocity: v

1 for k=1 to M do

2 \left|\begin{array}{ccc} \tilde{g_N} \leftarrow g_T + G_{NT}\lambda_T; \\ 3 & \lambda_N \leftarrow \arg\min_{\lambda \geq 0} \frac{1}{2}\lambda^\top G_N\lambda + \tilde{g_N}^\top \lambda; \\ 4 & \tilde{g_T} \leftarrow g_T + G_{TN}\lambda_N; \\ 5 & \lambda_T \leftarrow \arg\min_{\|\lambda^{(i)}\| \leq \mu_i \lambda_N^{(i)}} \frac{1}{2}\lambda^\top G_T\lambda + \tilde{g_T}^\top \lambda; \\ 6 \text{ end} \end{array}\right|
```

primal (*i.e.*, contact forces) and dual (*i.e.* contact velocities) variables but also the proximal parameter can be initialized with the previous values.

In addition, second-order algorithms can further exploit the recent progress in rigid body algorithms [43]. This work takes advantage of the sparse structure of the kinematic chains in order to efficiently compute the Cholesky decomposition of the Delassus matrix G. This approach is robust enough to handle the case of hyperstatic systems and reduces the cost of the computation of matrix-vector products involving G^{-1} (Alg. 3, line 3). This also indicates that evaluating G from its Cholesky decomposition, as required by per-contact approaches, actually constitutes an additional cost. In the context of ADMM (Alg. 3, the algorithm from [43] can also be favorably combined with the adaptation of the proximal parameter [68]. Indeed, updating the regularized Cholesky can be done at almost no cost by using [43].

Additionally, over-relaxation is often employed to accelerate the convergence of both Gauss-Seidel or ADMM algorithms. This technique applies the following update:

$$\lambda \leftarrow \alpha \lambda^- + (1 - \alpha)\lambda,\tag{22}$$

where $\alpha \in]0,2[$ and λ^- denotes the previous iteration. For $\alpha > 1$, over-relaxing consists in an extrapolation step and should be carefully used as it may also hinder convergence.

IV. EXPERIMENTS

In this section, we thoroughly evaluate the performances and behaviors of the formulations explained in Sec. III. To fairly compare and benchmark the various algorithmic formulations, we have implemented them in a unified C++ framework called ContactBench. This framework extensively relies on the Pinocchio library [24] for rigid body algorithms and HPP-FCL [38], [46] implementation of GJK and EPA for collision detection. It is worth noting that some popular simulators have closed-source implementations, such as RaiSim [33]. In this case, we strove to keep our implementation as close as possible to the information in the corresponding papers. ContactBench will be released as open-source upon article acceptance.

Several factors may hinder the correctness and accuracy of simulators based on time-stepping methods:

- i) the low accuracy of the solver of the contact problem;
- ii) the limitation from the contact model itself;
- or the numerical integration due to the time discretization scheme.

In this section, we first evaluate the error from sources i) and ii) (Sec. IV-A). The source of error i) is evaluated by measuring the time taken to reach a given accuracy. The errors from ii) are analyzed by measuring the residual for an (approximately) infinite time budget. We further assess i) and iii) by examining the sensitivity of the contact solvers with respect to respectively the stopping criterion value ϵ_{abs} and the time-step Δt (Sec. IV-B). Sec. IV-C evaluates their computational efficiency. Eventually, Sec. IV-D explores how the contact models and their implementations can impact the final robotics applications, in the case of the MPC for quadruped locomotion.

A. Evaluation of physical correctness

LCP relaxation. The linearization of the friction cone loses the isotropy and biases the friction forces towards some specific directions, as shown in Fig. 6). This observation has already been raised in the litterature [6], [8]. As expected, the bias on the contact forces significantly impairs the simulation by deviating the trajectory of the simulated system (Fig. 9).

CCP relaxation. As detailed previously, the CCP contact model relaxes the *Signorini condition*. As shown in Fig. 10, this results in non-null normal contact forces and velocities when a contact point is sliding. As a consequence, the contact points start to bump, which modifies the trajectory of the system (Fig. 10, left), which also impacts the overall dissipated

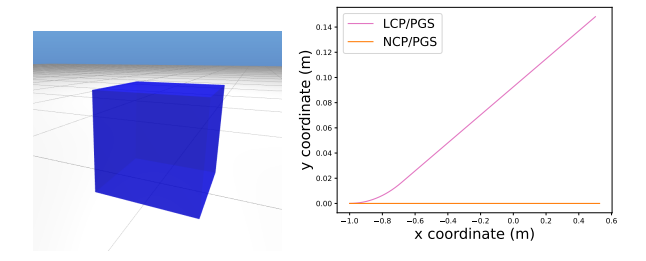


Fig. 9. **Trajectory of a cube sliding on a plane.** The cube is initialized with an initial tangential velocity along the y-axis. **Right:** The bias of friction forces (Fig.6) introduces a tangential velocity along the x-axis, which deviates the cube from the expected straight-line trajectory.

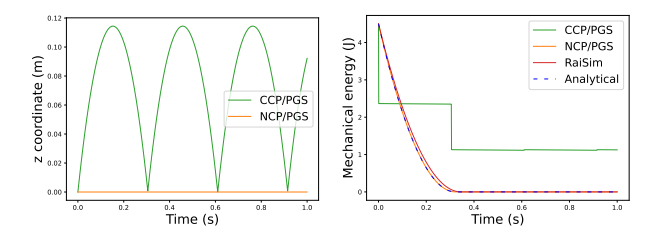


Fig. 10. A cube is initialized on a plane with a tangential velocity along the y-axis, similarly to the case studied in Fig. 9. Left: The CCP contact model relaxes the Signorini condition, which induces unphysical forces leading to the vertical bouncing of the cube. Right: From the MDP, it is possible to determine the evolution of the energy of the system analytically and compare it to what is computed by the various simulation algorithms. The CCP relaxation induces a significant gap with the analytical solution. The RaiSim contact model narrows this gap but dissipates less power than expected, as it does not enforce the MDP. The NCP formulation, solved using the PGS solver, is the only formulation which closely matches the expected analytical behavior of the system.

energy (Fig. 10, right). The model adopted by Raisim aims at correcting this undesired phenomenon by enforcing the Signorini condition but still does not match the analytical solution due to its relaxation of the MDP (21) (Fig. 10, right).

Underdetermined contact problems. Underdetermination occurs when infinite combinations of contact forces lead to the same trajectory. These artifacts happen on the normal and tangential components of contact forces, as depicted in Fig. 11. As shown in Fig. 11, the solution found depends on the numerical scheme. We observe that the per-contact approaches (Alg. 2,4 and 5) exhibit spurious internal forces at stiction, values which are not controlled by the algorithms. On the opposite, the algorithms working directly on the global contact problem with a proximal regularization (Alg. 3 and 6) avoid injecting such artifacts in the contact forces (Fig. ,11).

This phenomenon may seem innocuous as forward dynamics are not affected. However, it makes the inverse dynamics illposed, as there is no way to predict such numerical artifacts. Additionally, in the context of differentiable physics, we believe these spurious contact forces may catastrophically impact the computation of derivatives, but we leave this study as a future work. Finally, it is worth mentioning that such under-determined cases are ubiquitous in robotics (e.g., legged robots making redundant contact with their environments).

Robustness to ill-conditioning contact problems. More

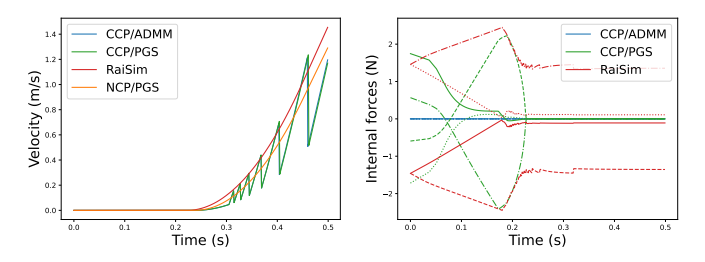


Fig. 11. Applying a linearly growing horizontal force to a cube on a plane. Left: The cube is at stiction before it starts sliding after approximately 0.25s. The tangential velocity differs depending on the contact model: CCP induces some bumps which occasionally dissipate energy during impacts, while RaiSim violates the MDP leading to contact points sliding faster than in the case of NCP. Right: At stiction, multiple combinations of tangential forces may lead to the same trajectory. There are four curves for each contact model, each curve accounting for one of the four contact forces on the cube. CCP solvers exhibit internal forces "stretching" the cube at stiction before the MDP enforces these forces to disappear when the cube starts to slide. RaiSim relaxes the maximum dissipation principle so the friction forces are not opposed to the movements, and internal forces persist when the cube is sliding. Eventually, ADMM avoids injecting spurious internal forces even at stiction.

generally, the contact problem becomes challenging when the ratio between the biggest and the smallest eigenvalue of the Delassus matrix grows. The experiment of Fig. 12 exhibits the convergence issues of per-contact approaches when simulating systems with a strong coupling between the different contact points, which causes large off-diagonal terms on the matrix G. Such a behavior can be expected as supposing the matrix to be diagonal dominant is a classical hypothesis ensuring the convergence of Gauss-Seidel methods. On the contrary, the proximal algorithms account for off-diagonal terms of G and only rely on a regularized inverse of G (Alg. 3, line 1) and thus robustly converge towards an optimal solution.

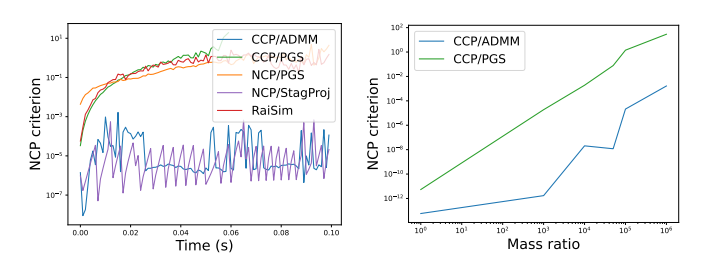


Fig. 12. Simulation of ill-conditioned systems. Left: Stacking a heavy cube $(10^3 \mathrm{kg})$ on a light one $(10^{-3} \mathrm{kg})$ makes the problem ill-conditioned and, therefore, not solvable via per-contact algorithms. **Right:** The accuracy of the simulators improves when the ratio between the masses of the two cubes gets close to one. The ADMM algorithm remains more accurate than PGS in all cases.

Effects of compliance. As demonstrated by Fig. 13, the normal forces vary linearly with the compliance parameter R. Moreover, adding compliance to the tangential components induces the vanishing of dry frictions, resulting in tangential oscillations instead of a null velocity. These compliant effects regularize the infinitely steep graphs due to the Signorini condition and Coulomb's law and replace them with locally linear mapping, which also eases the numerics. Therefore, the compliance added in MuJoCo has no physical purpose and should be considered a numerical trick designed to circumvent

the issues due to hyper-staticity or ill-conditioning at the cost of impairing the simulation.

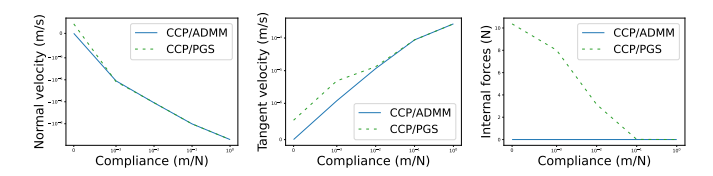


Fig. 13. Simulation of Solo-12 with varying compliance for the contacts with the floor. Left: Adding a compliance to the contact model relaxes both the Signorini condition. Center: This compliance also relaxes the Coulomb's law of friction. Right: Compliance also regularizes the problem, removing the spurious internal forces in under-determined cases.

B. Self-consistency of the solvers

The accuracy of simulators can be affected by the numerical resolution induced by two "hyper-parameters": the value of the stopping criterion for the contact solver desired accuracy (ϵ_{abs}) and the time-step value (Δt) . We measure their effect on the simulation quality when varying them independently. A simulator is said to be self-consistent when this deviation remains limited.

Time stepping. As already mentioned, time-stepping simulators are sensitive to the choice of the time-step Δt . Here, we intend to assess the self-consistency of the various contact solvers by examining their deviation when Δt grows. Because time discretization also affects the collision detection process, our study is done on the trajectory of a cube sliding on a plane whose contact points should remain constant. A trajectory obtained by simulating the system with a small time-step $(\Delta t = 0.1ms)$ serves as a reference to compute the state consistency error along the trajectories simulated with larger time-steps (Tab. III).

Solver	Time-step (ms)	Integral consistency error (m.s)
CCP/PGS	1	1.6×10^{-3}
CCP/PGS	10	1.0×10^{-2} 1.7×10^{-2}
CCP/PGS	100	1.6×10^{-1}
RaiSim	1	1.5×10^{-3}
RaiSim	10	1.6×10^{-2}
RaiSim	100	1.5×10^{-1}
NCP/PGS	1	1.5×10^{-3}
NCP/PGS	10	1.6×10^{-2}
NCP/PGS	100	1.6×10^{-1}

Looking at Tab. III, we observe that the sensitivities with respect to the time-step are similar for the various solvers. Moreover, as shown by Fig. 14, the energy evolution of the system simulated via NCP and RaiSim models is only a little affected when increasing Δt . On the contrary, the CCP relaxes the *Signorini condition*, which results in the cube taking off and causing a nonphysical and inconsistent evolution of the mechanical energy.

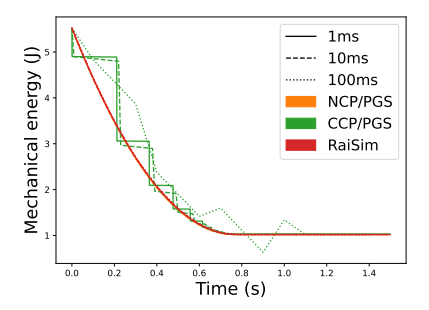


Fig. 14. Self-consistency w.r.t. time-stepping when simulating a cube initialized on a plane with a tangential velocity. The sensitivity to the time-stepping can also be observed through the evolution of mechanical energy.

Stopping criterion. As done in the case of the time-stepping, the sensitivity to the stopping criterion is evaluated by measuring the integrated consistency error with respect to a high-resolution ($\epsilon_{abs}=10^{-9}$) reference trajectory (Tab. IV). Contrarily to the time-stepping case, the solvers appear to have different behaviors when their stopping criteria are modified. Indeed, trajectories generated via the RaiSim and CCP contact models are significantly modified when ϵ_{abs} is increased (Tab. IV, Fig. 15). The figure 15 demonstrates that the NCP model simulates robustly the mechanical energy evolution, which is not true for the CCP and RaiSim models. In particular, as the accuracy of RaiSim is relaxed, due to its approximation (21), the error on the MDP becomes completely uncontained leading to almost no energy dissipation for low accuracies ($\epsilon_{abs}=10^{-2}$).

Solver	Stopping criterion	Integral consistency error (m.s)
CCP/PGS	10^{-6}	6.7×10^{-7}
CCP/PGS	10^{-4}	4.3×10^{-5}
CCP/PGS	10^{-2}	4.8×10^{-2}
RaiSim	10^{-6}	9.0×10^{-8}
RaiSim	10^{-4}	4.8×10^{-5}
RaiSim	10^{-2}	7.0×10^{-4}
NCP/PGS	10^{-6}	6.0×10^{-10}
NCP/PGS	10^{-4}	9.9×10^{-8}
NCP/PGS	10^{-2}	5.3×10^{-6}

C. Performance benchmarks

As evoked earlier, in addition to being physically accurate, it is also essential for a simulator to be fast, which, in general, constitutes two adversarial requirements. To evaluate the computational footprint of the various solvers, we measure the time taken to reach a fixed accuracy on dynamic trajectories involving robotics systems (Fig. 8). When the contact solvers are cold started, we observe that the second-order optimization techniques like ADMM are less efficient than the PGS solvers and their cheap per-contact iterations (Fig. 16, left). However, leveraging the solution from the previous time step to warmstart the solvers, a common strategy in practice, allows for

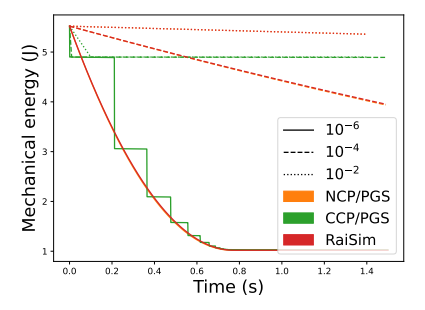


Fig. 15. Self-consistency w.r.t. stopping criteria when simulating a cube initialized on a plane with a tangential velocity. Dropping the solver accuracy hardly affect the energy evolution when using NCP/PGS. On the contrary, the energy of trajectories from the CCP/PGS and RaiSim algorithms is spectacularily impacted.

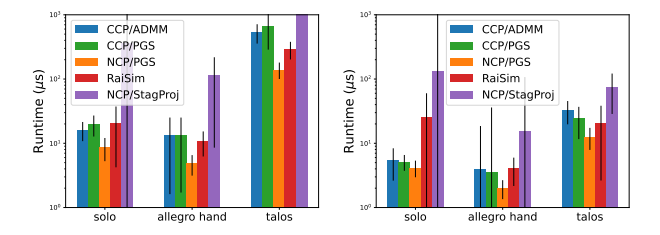


Fig. 16. Computational timings measured along a trajectory for three robotics systems (c.f. Fig. 8). Solo-12 and Talos are perturbed by applying an external force at their center of mass, while a ball is dropped in the Allegro hand, so the trajectories are not static. The contact solvers are tested in both cold-start (Left) and warm-start (Right) modes. We simulate the same trajectories to evaluate the benefit of warm-starting, but we use the solution of the previous time step as an initial guess. This leads to significant improvements in the computational timings.

significantly reducing this gap (Fig. 16, right). Therefore, regarding the study of Sec. IV-A, a trade-off appears for algorithms like ADMM and Staggered Projections, which treat all the contact points globally. In practice, they might be slower than their PGS counterpart while they benefit from better behaviors on ill-conditioned problems.

D. MPC for quadruped locomotion

The previous examples already illustrate the differences among the various simulators in terms of both physical accuracy and numerical efficiency. However, such scenarios may not represent the richness of contacts in practical robotics situations. For this purpose, we use the implementation of MPC on the Solo-12 system introduced in [69] to generate locomotion trajectories on flat and bumpy terrains. These experiments are designed to involve a wide variety of contacts (*i.e.*, sticking, sliding, and taking-off) and see how the simulation choices impact the final task (*i.e.*, horizontal translation of the robot).

For a flat and barely slippery ($\mu=0.9$) ground, we observe that the choice of simulator hardly affects the base velocity tracked by the MPC controller (Fig. 16, top right). In this case, the contacts are mainly sticking, leading to low violation of the NCP criterion (14) (Fig. 16, bottom left).

When the terrain is bumpy (roughness of $10^{-1}m$) and slippery ($\mu = 0.3$), the locomotion velocity generated from the RaiSim and CCP models significantly deviates from the NCP

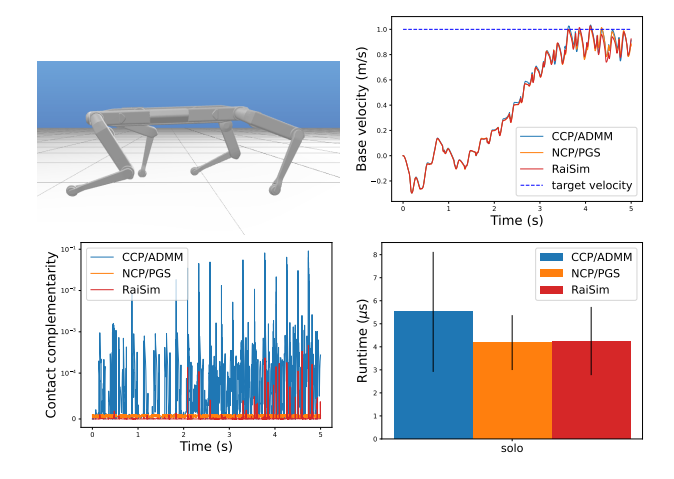


Fig. 17. MPC for locomotion on a flat terrain (Top left). The target horizontal translation velocity of the base is similarly reached by the controller with the different simulators (Top right). However, they do not equally respect the contact complementarity criterion is not (Bottom left). Per-contact approaches, e.g. are more efficient (Bottom right).

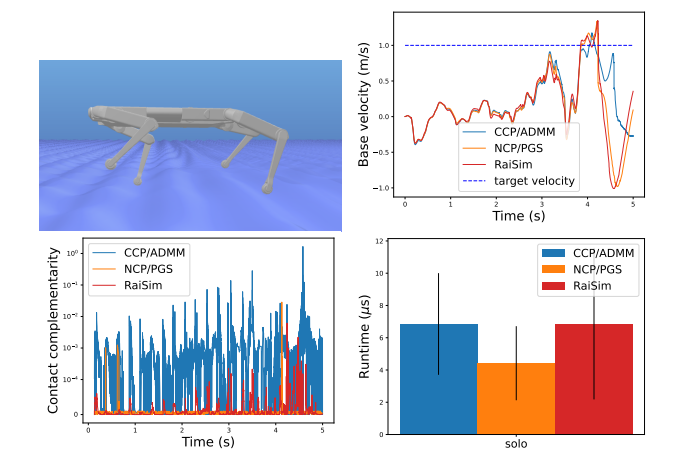


Fig. 18. MPC for locomotion on a bumpy terrain (Top left). The tracked velocity of the base quickly differs depending on the used simulator (Top right). Slippery contact points violate the contact complementarity criterion for the RaiSim and CCP contact modelings (Bottom left). The complexity of contacts also hampers the solvers and reduces the gap between per-contact and ADMM approaches (Bottom right).

one (Fig. 16, top right). This can be explained in the light of our previous study as both the RaiSim and CCP contact models make physical approximations when contact points are sliding (Fig. 16, bottom left) In addition, the simulation is more challenging than the flat case, which causes increased computations from the solvers, particularly for RaiSim (Fig. 16, bottom right). These observations indicate that the low-level choices of the contact solver may induce significant differences in the high-level behaviors of locomotion controllers on complex terrains.

V. DISCUSSION AND CONCLUSION

NCP is known to be complex to solve and thus is often relaxed to find approximate solutions. In this article, we report a deeper study on how the various rigid contact models commonly employed in robotics and their associated solvers can impact the resulting simulation. We have notably established and experimentally highlighted that these choices may induce unphysical artifacts, thus widening the reality gap, leading to unrealistic behaviors when the simulator is later used for practical robotics applications. Our experiments show that there is no fully satisfactory approach at the moment, as all existing solutions compromise either accuracy, robustness, or efficiency. This also indicates that there may still be room for improvements in contact simulation.

Beyond contact simulation, differentiable physics constitutes an emergent and closely related topic. However, the impact of forward simulation artifacts on gradient computation remains unexplored. In particular, some of the relaxations at work, e.g. the artificial compliance added in MuJoCo, result in crucial differences in gradients, which then affect downstream applications like trajectory optimization [70], [71]. We leave the study of the various existing differentiable simulators [5], [6], [7], [72], [8] through this lens as a future work.

For all these reasons, we believe it would be highly beneficial for the robotics community to take up such low-level topics around simulation, as they could lead to substantial progress in the field. The work of [36] is an inspiring first step in this direction. With this article, we intend to go further by providing open-source implementations and benchmarks to the community.

ACKNOWLEDGMENTS

We thank Jemin Hwangbo for providing useful details on the algorithm of the RaiSim simulator, and Stephane Caron for helpful discussions. This work was supported in part by L'Agence d'Innovation Défense, the French government under the management of Agence Nationale de la Recherche through the project INEXACT (ANR-22-CE33-0007-01) and as part of the "Investissements d'avenir" program, reference ANR-19-P3IA-0001 (PRAIRIE 3IA Institute), by the European Union through the AGIMUS project (GA no.101070165) and the Louis Vuitton ENS Chair on Artificial Intelligence. Views and opinions expressed are those of the author(s) only and do not necessarily reflect those of the European Union or the European Commission. Neither the European Union nor the European Commission can be held responsible for them.

REFERENCES

- [1] W. Li and E. Todorov, "Iterative linear quadratic regulator design for nonlinear biological movement systems.," vol. 1, pp. 222-229, 01 2004.
- [2] D. Mayne, "A second-order gradient method for determining optimal trajectories of non-linear discrete-time systems," International Journal of Control, vol. 3, no. 1, pp. 85-95, 1966.
- [3] Y. Tassa, T. Erez, and E. Todorov, "Synthesis and stabilization of complex behaviors through online trajectory optimization," in 2012 IEEE/RSJ International Conference on Intelligent Robots and Systems, pp. 4906-4913, IEEE, 2012.
- [4] J. Carpentier and N. Mansard, "Analytical derivatives of rigid body dynamics algorithms," in Robotics: Science and systems (RSS 2018),
- [5] F. de Avila Belbute-Peres, K. Smith, K. Allen, J. Tenenbaum, and J. Z. Kolter, "End-to-end differentiable physics for learning and control," Advances in neural information processing systems, vol. 31, 2018.
- [6] Q. Le Lidec, I. Kalevatykh, I. Laptev, C. Schmid, and J. Carpentier, 'Differentiable simulation for physical system identification,' Robotics and Automation Letters, vol. 6, no. 2, pp. 3413-3420, 2021.

- [7] K. Werling, D. Omens, J. Lee, I. Exarchos, and C. K. Liu, "Fast and feature-complete differentiable physics engine for articulated rigid bodies with contact constraints," in Robotics: Science and Systems, 2021.
- T. Howell, S. Le Cleac'h, J. Brüdigam, Z. Kolter, M. Schwager, and Z. Manchester, "Dojo: A differentiable simulator for robotics," arXiv preprint arXiv:2203.00806, 2022.
- M. Diehl, H. G. Bock, H. Diedam, and P.-B. Wieber, "Fast direct multiple shooting algorithms for optimal robot control," in Fast motions in biomechanics and robotics, pp. 65-93, Springer, 2006.
- [10] D. Q. Mayne, "Model predictive control: Recent developments and future promise," Automatica, vol. 50, no. 12, pp. 2967–2986, 2014.
- [11] S. Kleff, A. Meduri, R. Budhiraja, N. Mansard, and L. Righetti, "Highfrequency nonlinear model predictive control of a manipulator," in 2021 IEEE International Conference on Robotics and Automation (ICRA), pp. 7330-7336, IEEE, 2021.
- [12] E. Dantec, M. Taix, and N. Mansard, "First order approximation of model predictive control solutions for high frequency feedback," IEEE Robotics and Automation Letters, vol. 7, no. 2, pp. 4448-4455, 2022.
- [13] R. S. Sutton and A. G. Barto, Reinforcement learning: An introduction. MIT press, 2018.
- [14] J. Tan, T. Zhang, E. Coumans, A. Iscen, Y. Bai, D. Hafner, S. Bohez, and V. Vanhoucke, "Sim-to-real: Learning agile locomotion for quadruped robots.," in Robotics: Science and Systems, 2018.
- [15] I. Akkaya, M. Andrychowicz, M. Chociej, M. Litwin, B. McGrew, A. Petron, A. Paino, M. Plappert, G. Powell, R. Ribas, et al., "Solving rubik's cube with a robot hand," arXiv preprint arXiv:1910.07113, 2019.
- J. Hwangbo, J. Lee, A. Dosovitskiy, D. Bellicoso, V. Tsounis, V. Koltun, and M. Hutter, "Learning agile and dynamic motor skills for legged robots," Science Robotics, vol. 4, no. 26, p. eaau5872, 2019.
- M. T. Mason and J. K. Salisbury Jr, Robot hands and the mechanics of manipulation. The MIT Press, Cambridge, MA, 1985.
- [18] J. Ponce, S. Sullivan, A. Sudsang, J.-D. Boissonnat, and J.-P. Merlet, "On computing four-finger equilibrium and force-closure grasps of polyhedral objects," The International Journal of Robotics Research, vol. 16, no. 1, pp. 11-35, 1997.
- [19] B. Dynamics, "Atlas gets a grip | boston dynamics." https://youtu.be/ -e1_QhJ1EhQ.
- [20] I. Mordatch, E. Todorov, and Z. Popović, "Discovery of complex behaviors through contact-invariant optimization," ACM Transactions on Graphics (ToG), vol. 31, no. 4, pp. 1-8, 2012.
- [21] M. Posa, C. Cantu, and R. Tedrake, "A direct method for trajectory optimization of rigid bodies through contact," The International Journal of Robotics Research, vol. 33, no. 1, pp. 69-81, 2014.
- [22] M. A. Toussaint, K. R. Allen, K. A. Smith, and J. B. Tenenbaum, "Differentiable physics and stable modes for tool-use and manipulation planning," 2018.
- [23] R. Featherstone, Rigid body dynamics algorithms. Springer, 2014.
- [24] J. Carpentier, G. Saurel, G. Buondonno, J. Mirabel, F. Lamiraux, O. Stasse, and N. Mansard, "The pinocchio c++ library: A fast and flexible implementation of rigid body dynamics algorithms and their analytical derivatives," in 2019 IEEE/SICE International Symposium on System Integration (SII), pp. 614-619, IEEE, 2019.
- [25] J. J. Moreau, "Unilateral Contact and Dry Friction in Finite Freedom Dynamics," in Nonsmooth Mechanics and Applications (M. J.J. and P. P.D., eds.), vol. 302 of International Centre for Mechanical Sciences (Courses and Lectures), pp. 1-82, Springer, 1988.
- [26] M. Jean, "The non-smooth contact dynamics method," Computer methods in applied mechanics and engineering, vol. 177, no. 3-4, pp. 235-257,
- V. Acary, F. Cadoux, C. Lemaréchal, and J. Malick, "A formulation of the linear discrete Coulomb friction problem via convex optimization," Journal of Applied Mathematics and Mechanics / Zeitschrift für Angewandte Mathematik und Mechanik, vol. 91, pp. 155-175, Feb. 2011.
- [28] B. Brogliato, A. Ten Dam, L. Paoli, F. Génot, and M. Abadie, "Numerical simulation of finite dimensional multibody nonsmooth mechanical systems," *Appl. Mech. Rev.*, vol. 55, no. 2, pp. 107–150, 2002. [29] R. Smith, "Open dynamics engine," 2008. http://www.ode.org/.
- [30] E. Coumans and Y. Bai, "Pybullet, a python module for physics simulation for games, robotics and machine learning." http://pybullet.org, 2016-2021.
- J. Lee, M. X. Grey, S. Ha, T. Kunz, S. Jain, Y. Ye, S. S. Srinivasa, M. Stilman, and C. K. Liu, "DART: Dynamic animation and robotics toolkit," The Journal of Open Source Software, vol. 3, p. 500, Feb 2018.
- E. Todorov, T. Erez, and Y. Tassa, "Mujoco: A physics engine for modelbased control," in 2012 IEEE/RSJ international conference on intelligent robots and systems, pp. 5026-5033, IEEE, 2012.
- [33] J. Hwangbo, J. Lee, and M. Hutter, "Per-contact iteration method for solving contact dynamics," IEEE Robotics and Automation Letters, vol. 3, no. 2, pp. 895-902, 2018.

- [34] D. M. Kaufman, S. Sueda, D. L. James, and D. K. Pai, "Staggered projections for frictional contact in multibody systems," pp. 1–11, 2008.
- [35] T. Erez, Y. Tassa, and E. Todorov, "Simulation tools for model-based robotics: Comparison of bullet, havok, mujoco, ode and physx," in 2015 IEEE International Conference on Robotics and Automation (ICRA), pp. 4397–4404, 2015.
- [36] P. Horak and J. C. Trinkle, "On the similarities and differences among contact models in robot simulation," *IEEE Robotics and Automation Letters*, vol. 4, pp. 493–499, 2019.
- [37] J. Carpentier, F. Valenza, N. Mansard, et al., "Pinocchio: fast forward and inverse dynamics for poly-articulated systems." https://stack-oftasks.github.io/pinocchio, 2015–2021.
- [38] J. Pan, S. Chitta, D. Manocha, F. Lamiraux, J. Mirabel, J. Carpentier, et al., "HPP-FCL: an extension of the Flexible Collision Library." https://github.com/humanoid-path-planner/hpp-fcl, 2015–2022.
- [39] J. Mirabel, S. Tonneau, P. Fernbach, A.-K. Seppälä, M. Campana, N. Mansard, and F. Lamiraux, "HPP: A new software for constrained motion planning," in *International Conference on Intelligent Robots and Systems*, 2016.
- [40] L. Montaut, Q. Le Lidec, V. Petrík, J. Sivic, and J. Carpentier, "Collision Detection Accelerated: An Optimization Perspective," in *Proceedings of Robotics: Science and Systems*, (New York City, NY, USA), June 2022.
- [41] P.-L. M. de Maupertuis, Essais de cosmologie. 1751.
- [42] S. L. Campbell and C. W. Gear, "The index of general nonlinear daes," Numerische Mathematik, vol. 72, pp. 173–196, 1995.
- [43] J. Carpentier, R. Budhiraja, and N. Mansard, "Proximal and sparse resolution of constrained dynamic equations," in *Robotics: Science and Systems*, 2021.
- [44] C. F. Gauß, "Über ein neues allgemeines grundgesetz der mechanik.," 1829.
- [45] F. E. Udwadia and R. E. Kalaba, "A new perspective on constrained motion," Proceedings of the Royal Society of London. Series A: Mathematical and Physical Sciences, vol. 439, no. 1906, pp. 407–410, 1992.
- [46] L. Montaut, Q. Le Lidec, V. Petrik, J. Sivic, and J. Carpentier, "Collision detection accelerated: An optimization perspective," in RSS 2022-Robotics: Science and Systems, 2022.
- [47] E. G. Gilbert, D. W. Johnson, and S. S. Keerthi, "A fast procedure for computing the distance between complex objects in three-dimensional space," *IEEE Journal on Robotics and Automation*, vol. 4, no. 2, pp. 193– 203, 1988.
- [48] C. Ericson, Real-Time Collision Detection. The Morgan Kaufmann Series, 2004
- [49] A. Signorini, "Questioni di elasticità non linearizzata e semilinearizzata," Rendiconti di Matematica e delle sue applicazioni, vol. 18, no. 5, pp. 95– 139, 1959
- [50] R. W. Cottle, J.-S. Pang, and R. E. Stone, *The Linear Complementarity Problem*. Society for Industrial and Applied Mathematics, 2009.
- [51] P. Wensing, R. Featherstone, and D. E. Orin, "A reduced-order recursive algorithm for the computation of the operational-space inertia matrix," in 2012 IEEE International Conference on Robotics and Automation, pp. 4911–4917, IEEE, 2012.
- [52] J. Baumgarte, "Stabilization of constraints and integrals of motion in dynamical systems," Computer methods in applied mechanics and engineering, vol. 1, no. 1, pp. 1–16, 1972.
- [53] G. de Saxcé and Z.-Q. Feng, "The bipotential method: A constructive approach to design the complete contact law with friction and improved numerical algorithms," *Mathematical and Computer Modelling*, vol. 28, pp. 225–245, Aug. 1998.

- [54] V. Acary, M. Brémond, and O. Huber, "On solving contact problems with Coulomb friction: formulations and numerical comparisons," Research Report RR-9118, INRIA, Nov. 2017.
- [55] K. Erleben, "Rigid body contact problems using proximal operators," in *Proceedings of the ACM SIGGRAPH / Eurographics Symposium on Computer Animation*, SCA '17, (New York, NY, USA), Association for Computing Machinery, 2017.
- [56] J. Pan, S. Chitta, and D. Manocha, "FCL: A General Purpose Library for Collision and Proximity Queries," in 2012 IEEE International Conference on Robotics and Automation, IEEE, 2012.
- [57] D. Fiser, "libccd." https://github.com/danfis/libccd.
- [58] M. L. Felis, "Rbdl: an efficient rigid-body dynamics library using recursive algorithms," *Autonomous Robots*, vol. 41, no. 2, pp. 495–511, 2017
- [59] R. Tedrake and the Drake Development Team, "Drake: Model-based design and verification for robotics," 2019.
- [60] M. Macklin, K. Storey, M. Lu, P. Terdiman, N. Chentanez, S. Jeschke, and M. Müller, "Small steps in physics simulation," in *Proceedings of the 18th Annual ACM SIGGRAPH/Eurographics Symposium on Computer Animation*, SCA '19, (New York, NY, USA), Association for Computing Machinery, 2019.
- [61] M. Anitescu and A. Tasora, "An iterative approach for cone complementarity problems for nonsmooth dynamics," *Computational Optimization and Applications*, vol. 47, no. 2, pp. 207–235, 2010.
- [62] K. Erleben, "Numerical methods for linear complementarity problems in physics-based animation," in ACM SIGGRAPH 2013 Courses, SIGGRAPH '13, (New York, NY, USA), Association for Computing Machinery, 2013.
- [63] S. Boyd, N. Parikh, E. Chu, B. Peleato, J. Eckstein, et al., "Distributed optimization and statistical learning via the alternating direction method of multipliers," Foundations and Trends® in Machine learning, vol. 3, no. 1, pp. 1–122, 2011.
- [64] S. Mehrotra, "On the implementation of a primal-dual interior point method," SIAM Journal on optimization, vol. 2, no. 4, pp. 575–601, 1992.
- [65] T. Preclik, Models and algorithms for ultrascale simulations of nonsmooth granular dynamics. Friedrich-Alexander-Universitaet Erlangen-Nuernberg (Germany), 2014.
- [66] S. Boyd and L. Vandenberghe, "Localization and cutting-plane methods," From Stanford EE 364b lecture notes, 2007.
- [67] F. Jourdan, P. Alart, and M. Jean, "A gauss-seidel like algorithm to solve frictional contact problems," *Computer methods in applied mechanics* and engineering, vol. 155, no. 1-2, pp. 31–47, 1998.
- [68] R. Nishihara, L. Lessard, B. Recht, A. Packard, and M. Jordan, "A general analysis of the convergence of admm," in *International conference on machine learning*, pp. 343–352, PMLR, 2015.
- [69] P.-A. Léziart, T. Flayols, F. Grimminger, N. Mansard, and P. Souères, "Implementation of a Reactive Walking Controller for the New Open-Hardware Quadruped Solo-12," in 2021 IEEE International Conference on Robotics and Automation - ICRA, (Xi'an, China), May 2021.
- [70] H. J. T. Suh, T. Pang, and R. Tedrake, "Bundled gradients through contact via randomized smoothing," *IEEE Robotics and Automation Letters*, vol. 7, no. 2, pp. 4000–4007, 2022.
- [71] Q. Le Lidec, L. Montaut, C. Schmid, I. Laptev, and J. Carpentier, "Leveraging randomized smoothing for optimal control of nonsmooth dynamical systems," arXiv preprint arXiv:2203.03986, 2022.
- [72] E. Heiden, D. Millard, E. Coumans, Y. Sheng, and G. S. Sukhatme, "NeuralSim: Augmenting differentiable simulators with neural networks," in *Proceedings of the IEEE International Conference on Robotics and Automation (ICRA)*, 2021.